Dry Sliding Wear Behavior of In-Situ Al–Mg_2Si Metal Matrix Composites

Suresh K[1], Gangadhar Medleri[2], Shubha T C[1]

[1]Department of Mechanical Engineering, Government Engineering College, Talakal, Koppal,

(Affiliated to Visvesvaraya Technological University, Belagavi),

[2]Supinco Automation PVT LTD, Bengaluru

Abstract

The present study investigates the dry sliding wear behavior of in-situ synthesized Al–Mg_2Si metal matrix composites under low sliding velocity conditions. The composites were fabricated using the stir casting technique, ensuring uniform dispersion and strong interfacial bonding of Mg_2Si reinforcements within the aluminum matrix. Dry sliding wear tests were conducted using a pin-on-disc apparatus at a constant sliding velocity of 1 m/s under applied normal loads ranging from 10 N to 100 N. Cylindrical pin specimens of 8 mm and 10 mm diameters were evaluated to assess the influence of specimen geometry on wear behavior. The results reveal a monotonic increase in wear rate with applied load, while the specific wear rate remains nearly constant across the load range, indicating adherence to Archard's wear law. The coefficient of friction exhibits minimal sensitivity to load, confirming stable sliding conditions. Comparative analysis shows that the 10 mm diameter pins consistently demonstrate superior wear resistance due to reduced contact stress. The findings establish the suitability of in-situ Al–Mg_2Si composites for low-velocity, moderate-load tribological applications.

Keywords: Al–Mg_2Si composites; in-situ reinforcement; dry sliding wear; pin-on-disc; Archard's law

1. Introduction

Aluminium-based metal matrix composites (AMCs) have attracted extensive research interest owing to their high specific strength, low density, good thermal conductivity, and superior wear resistance, making them suitable for automotive and aerospace applications [1–3]. Among various reinforcement systems, in-situ formed intermetallic compounds have gained preference over ex-situ reinforcements due to their clean interfaces, fine particle size, and uniform distribution within the matrix [4–6].

Mg_2Si is a lightweight intermetallic compound with low density, high hardness, and good thermal stability, making it an attractive reinforcement for aluminum alloys [7–9]. In-situ formation of Mg_2Si within aluminum matrices eliminates wetting problems and particle clustering commonly observed in ex-situ composites, thereby enhancing mechanical and tribological performance [10–12]. Previous studies have reported improved hardness, stiffness, and wear resistance of Al–Mg_2Si composites compared to monolithic aluminum alloys [13–15].

Dry sliding wear behavior of AMCs is strongly influenced by applied load, sliding velocity, reinforcement characteristics, and contact geometry [16–18]. Several researchers have established that wear rate increases with load due to increased real area of contact and plastic deformation of surface asperities [19–21]. However, the specific wear rate often remains relatively constant when the dominant wear mechanism does not change, in accordance with Archard's wear theory [22–24].

Although numerous studies have investigated the wear behavior of Al–Mg_2Si composites, limited attention has been paid to the combined effect of pin geometry and low sliding velocity on wear performance. Low-velocity sliding conditions are particularly relevant to applications such as guide rails, bushings, and bearing components, where stable wear behavior and long service life are critical [25–27]. Furthermore, comparative studies addressing the influence of specimen diameter under identical testing conditions are scarce.

The present work aims to address this gap by systematically investigating the dry sliding wear behavior of in-situ Al–Mg_2Si composites at a constant sliding velocity of 1 m/s. The effect of applied load and pin diameter on wear rate, specific wear rate, coefficient of friction, and wear coefficient is analyzed, and the governing wear mechanisms are discussed.

2. Materials and Methods

2.1 Fabrication of Al–Mg_2Si Composites

In-situ Al–Mg_2Si metal matrix composites were fabricated using the stir casting technique. Commercially available aluminum was melted in an electric resistance furnace and superheated above its liquidus temperature. Predetermined amounts of magnesium and silicon were added to the molten aluminum to form Mg_2Si reinforcements in situ. Mechanical stirring was performed intermittently for 60 minutes to ensure uniform dispersion and near-spherical morphology of the Mg_2Si particles. The homogeneous melt was bottom-poured into a preheated graphite mold and allowed to solidify under controlled cooling conditions.

2.2 Specimen Preparation

Cylindrical pin specimens of 8 mm and 10 mm diameter were machined from the as-cast composite ingots. The pin length was maintained constant for all tests. Prior to wear testing, the pin surfaces were ground using emery papers of increasing grit size and polished to obtain a smooth and flat contact surface. All specimens were ultrasonically cleaned in acetone and dried to remove surface contaminants.

2.3 Wear Testing

Dry sliding wear tests were conducted using a pin-on-disc tribometer with EN31 steel as the counterface material. The specifications of the pin-on-disc tribometer employed in this study are summarized in Table 1.

Table 1: Pin-on-Disc Machine Specifications

Parameter	Units	Minimum	Maximum
Wear disc diameter	mm	165	---
Disc speed	rpm	50	3,000
Pin diameter	mm	8	10
Pin length	mm	30	50
Wear track diameter	mm	10	140
Normal load	N	10	200

Tests were performed under normal loads of 10–100 N at sliding velocity of 1 m/s, with a constant wear track diameter of 100 mm. Ambient test conditions were maintained at 28–32 °C and 50–60% relative humidity. Figure 1 shows the photograph of the wear testing facilities at the laboratory.

Figure 1: Photograph of the wear testing setup

2.4 Wear Measurement and Calculations

Wear was evaluated by measuring mass loss using a digital balance (±0.01 g accuracy). The wear rate, specific wear rate, coefficient of friction, and wear coefficient are evaluated by using standard tribological relations based on mass loss, sliding distance, applied load, and material hardness. After each wear test, specimens were carefully cleaned to remove loose debris and prevent

interference with subsequent measurements. Wear was initially evaluated in terms of mass loss (Δm), measured using a digital balance. The wear rate (W) was calculated as:

$$W = \frac{\Delta m}{L}$$

where Δm is the mass loss and $L$is the sliding distance.

The friction force (F_f) was continuously recorded during each test and averaged over the total number of passes. The coefficient of friction (μ) was determined using:

$$\mu = \frac{F_f}{F_n}$$

where F_n is the applied normal load.

To characterize the abrasive wear behavior more effectively, the specific wear rate was evaluated based on volumetric wear loss. The volumetric wear rate (W_v) was calculated as:

$$W_v = \frac{V}{L}$$

where $V$is the volume loss. The specific wear rate (W_s) was then determined as:

$$W_s = \frac{V}{L\,F_n}$$

Additionally, wear resistance was expressed as the inverse of wear rate. The wear coefficient (K) was calculated using:

$$K = \frac{V \times H}{F_n \times L}$$

where H is the hardness of the material.

Wear Calculation Procedure

- Cross-sectional area of pin: $A = \pi r^2$
- Volume loss: $V = A \times h$, where h is the height loss.
- Wear rate: $W = \frac{V}{L}$
- Wear resistance: $= \frac{1}{W}$
- Specific wear rate: $W_s = \frac{W}{F_n}$

3. Results and Discussion

This section presents a detailed analysis of the wear behavior of the composite by evaluating wear rate, specific wear rate, coefficient of friction, and dimensionless wear coefficient, and correlating these parameters with applied normal load under dry sliding conditions. The normal load was varied from 10 N to 100 N, and the initial and final weights of the specimens were measured to

determine weight loss and corresponding volume loss. Based on these measurements, the wear rate, specific wear rate, average frictional force, coefficient of friction, and wear coefficient were calculated.

3.1 Wear analysis of 8 mm diameter pin specimen

The following discussion focuses on the trends observed for the 8 mm diameter pin specimen tested at a sliding velocity of 1 m/s.

Figure 2 illustrates the variation of wear rate with applied load. As the load increased from 10 N to 100 N, the wear rate increased from 0.000981 mm^3/m to 0.004904 mm^3/m, exhibiting a nearly linear trend. This behavior can be attributed to the increase in real area of contact between the mating surfaces due to plastic deformation of surface asperities under higher normal loads. The increased real contact area results in higher interfacial shear stresses, which facilitate material removal from the comparatively softer matrix during sliding, leading to an increased wear rate.

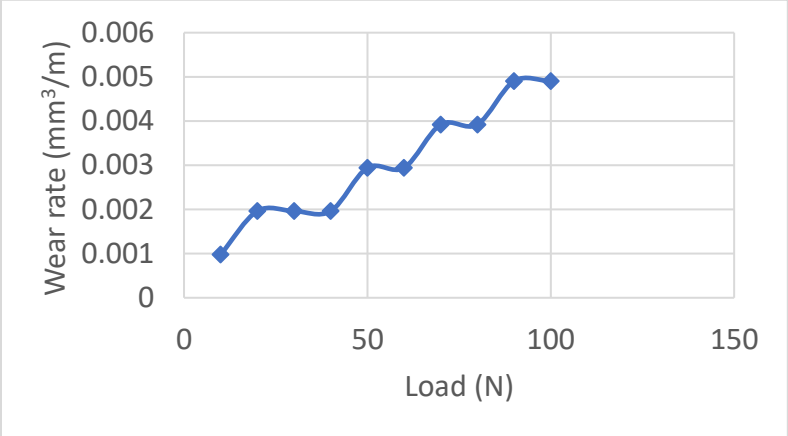

Figure 2: Wear rate vs load for 8 mm specimen at 1 m/s

The variation of specific wear rate with load is shown in Figure 3. At lower loads (10–20 N), the specific wear rate exhibits higher values, approximately 9.81×10^{-5} mm^3/Nm, which may be attributed to the initial running-in period characterized by unstable contact conditions and higher material removal. With further increase in load, the specific wear rate remains nearly constant, varying only between 4.9×10^{-5} and 6×10^{-5} mm^3/Nm up to 100 N. This behavior is consistent with Archard's wear law, which states that wear volume is directly proportional to the applied load under mild wear conditions. When the wear volume increases linearly with load, normalization with respect to load and sliding distance results in an approximately constant specific wear rate, indicating that the dominant wear mechanism remains unchanged within the investigated load range.

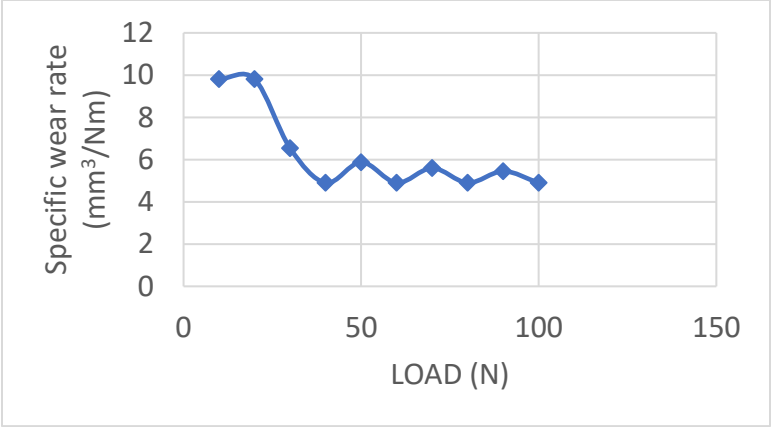

Figure 3: Specific wear rate vs load for 8 mm specimen at 1 m/s

Figure 4 presents the variation of the coefficient of friction with applied load. The coefficient of friction remains relatively stable, ranging from 0.47 to 0.57, with no significant dependence on load. This suggests the establishment of a steady-state sliding condition, possibly due to the formation of a stable mechanically mixed layer at the contact interface, which regulates frictional behavior despite increasing normal load.

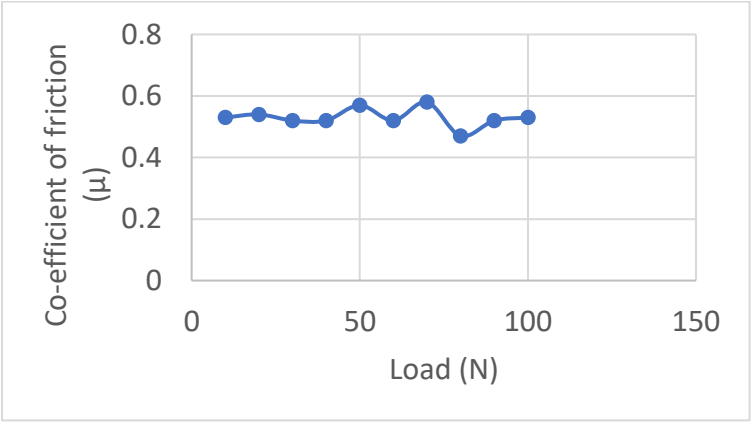

Figure 4: Co-efficient of friction vs load for 8 mm specimen at 1 m/s

The dimensionless wear coefficient as a function of load is shown in Figure 5. At lower loads (10–20 N), the wear coefficient exhibits higher values, approximately 6.64×10^{-5}, which may be attributed to the initial running-in period characterized by unstable contact conditions and higher material removal. With further increase in load, the wear coefficient decreases and stabilizes within the range of 3.32×10^{-5} to 3.98×10^{-5} up to 100 N. This stabilization indicates the transition to a steady wear regime, where improved load-bearing capacity of the composite and stabilization of the tribolayer contribute to controlled and predictable wear behavior.

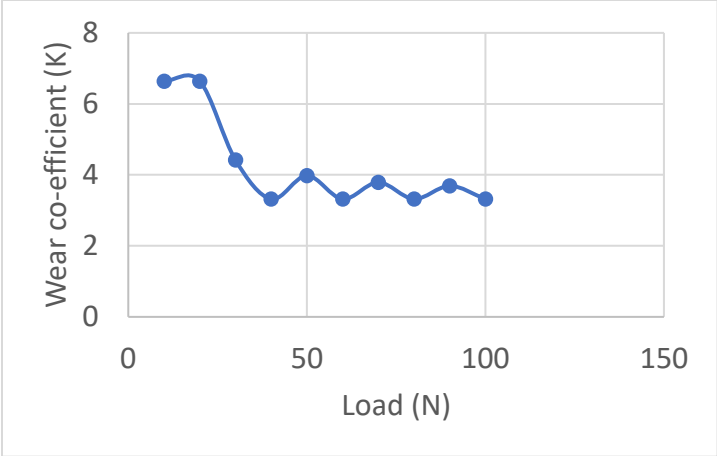

Figure 5: Wear co-efficient vs load for 8 mm specimen at 1 m/s

3.2 Wear analysis of 10 mm diameter pin specimen

The following discussion focuses on the trends observed for the 10 mm diameter pin specimen tested at a sliding velocity of 1 m/s.

Figure 6 illustrates the variation of wear rate with applied load. As the load increased from 10 N to 100 N, the wear rate increased from 0.000985 mm^3/m to 0.003941 mm^3/m, exhibiting a nearly linear trend. This behavior can be attributed to the increase in real area of contact between the mating surfaces due to plastic deformation of surface asperities under higher normal loads. The increased real contact area results in higher interfacial shear stresses, which facilitate material removal from the comparatively softer matrix during sliding, leading to an increased wear rate.

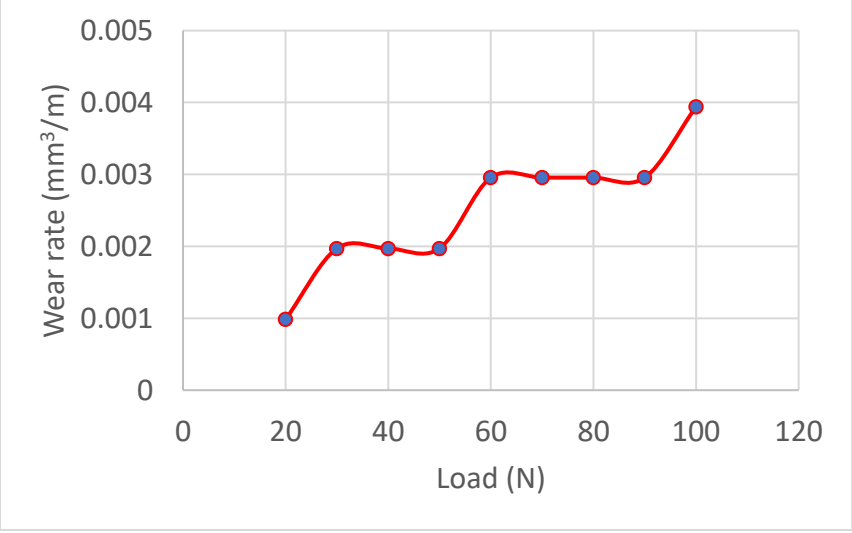

Figure 6: Wear rate vs load for 10 mm specimen at 1 m/s

The variation of specific wear rate with load is shown in Figure 7. Despite the increase in wear rate with load, the specific wear rate remains nearly constant, varying only between 6.56×10^{-5}

and 3.28×10^{-5} mm³/Nm over the entire load range. This behavior is consistent with Archard's wear law, which states that wear volume is directly proportional to the applied load under mild wear conditions. When the wear volume increases linearly with load, normalization with respect to load and sliding distance results in an approximately constant specific wear rate, indicating that the dominant wear mechanism remains unchanged within the investigated load range.

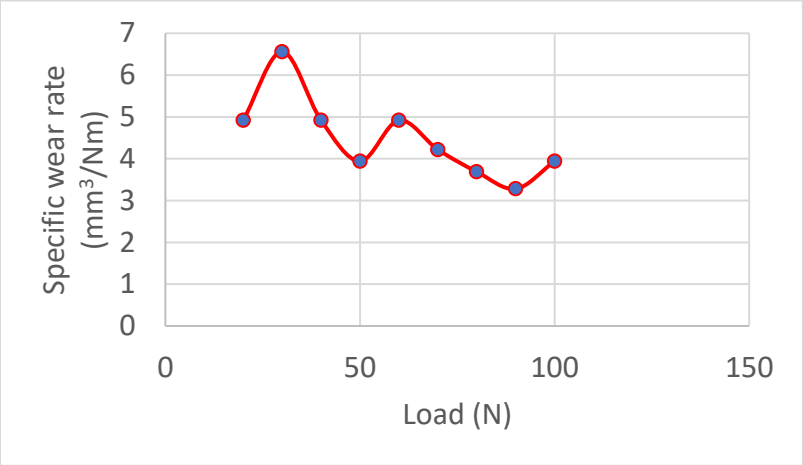

Figure 7: Specific wear rate vs load for 10 mm specimen at 1 m/s

Figure 8 presents the variation of the coefficient of friction with applied load. The coefficient of friction remains relatively stable, ranging from 0.49 to 0.65, with no significant dependence on load. This suggests the establishment of a steady-state sliding condition, possibly due to the formation of a stable mechanically mixed layer at the contact interface, which regulates frictional behavior despite increasing normal load.

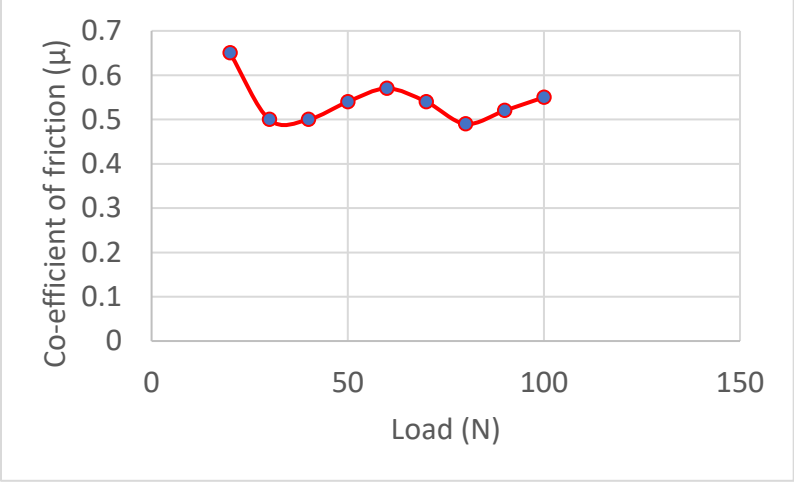

Figure 8: Co-efficient of friction vs load for 10 mm specimen at 1 m/s

The dimensionless wear coefficient as a function of load is shown in Figure 9. At lower loads (10–20 N), the wear coefficient exhibits higher values, approximately 4.44×10^{-5}, which may be attributed to the initial running-in period characterized by unstable contact conditions and higher

material removal. With further increase in load, the wear coefficient decreases and stabilizes within the range of 2.22×10^{-5} to 3.33×10^{-5} up to 100 N. This stabilization indicates the transition to a steady wear regime, where improved load-bearing capacity of the composite and stabilization of the tribolayer contribute to controlled and predictable wear behavior.

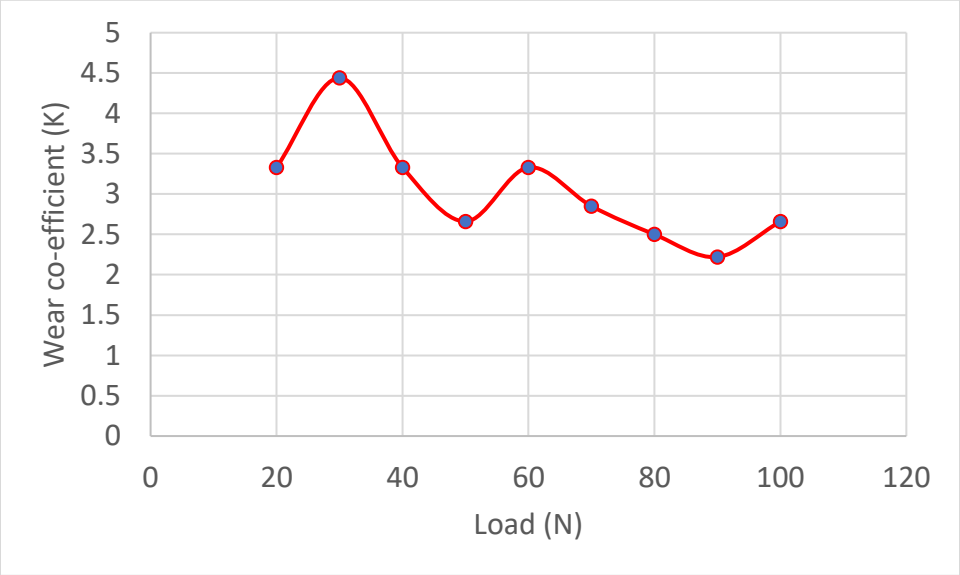

Figure 9: Wear co-efficient vs load for 10 mm specimen at 1 m/s

3.3 Comparative Discussion of Wear Parameters for 8 mm and 10 mm Diameter Pin Specimens

A comparative assessment of the tribological performance of 8 mm and 10 mm diameter pin specimens was carried out at a constant sliding velocity of 1 m/s under applied loads ranging from 10 N to 100 N. The superimposed variation of wear rate with load for both pin diameters is presented in Figure 10. For both specimens, the wear rate increased monotonically with increasing load; however, the 8 mm diameter pin consistently exhibited higher wear rates than the 10 mm pin across the entire load range. At the maximum load of 100 N, the wear rate of the 8 mm pin reached approximately 4.9×10^{-3} mm³/m, whereas the corresponding value for the 10 mm pin was lower, around 3.9×10^{-3} mm³/m. This difference is primarily attributed to the larger nominal contact area of the 10 mm pin, which reduces contact pressure and limits plastic deformation and micro-cutting at the sliding interface.

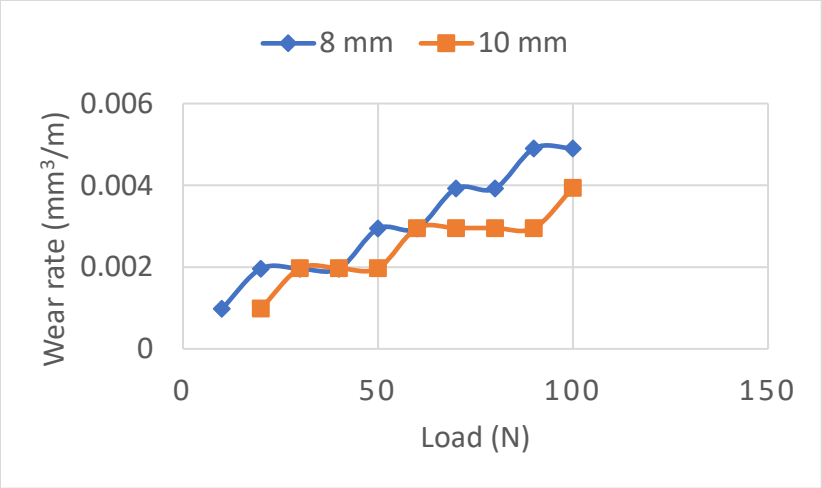

Figure 10: Comparison of wear rate vs load for 10 mm specimen at 1 m/s

The superimposed plot of specific wear rate as a function of load for both pin diameters is shown in Figure 11. Despite the increase in absolute wear rate with load, the specific wear rate remained nearly constant for both specimens, varying within the range of approximately (3–10) × 10^{-5} mm^3/Nm. For example, in the case of the 8 mm pin, the specific wear rate decreased slightly from about 9.8 × 10^{-5} mm^3/Nm at 20 N to 3.9 × 10^{-5} mm^3/Nm at 100 N, while the 10 mm pin consistently exhibited marginally lower values at corresponding loads. This near load-independent behavior confirms adherence to Archard's wear law and indicates that the dominant wear mechanism remains stable and unchanged for both pin geometries within the investigated load range.

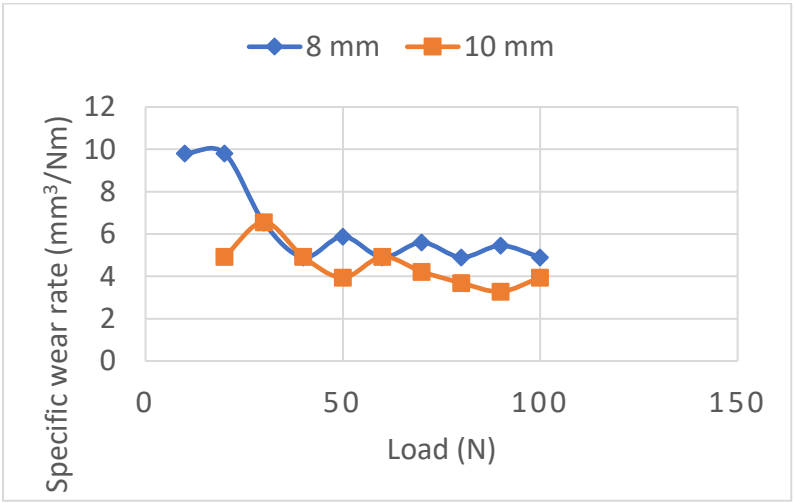

Figure 11: Comparison of specific wear rate vs load for 10 mm specimen at 1 m/s

The variation of coefficient of friction with applied load for both pin diameters is illustrated in Figure 12. For both specimens, the coefficient of friction remained relatively constant with increasing load, indicating steady-state sliding conditions. The 8 mm pin showed coefficient of friction values in the range of approximately 0.47–0.58, while the 10 mm pin exhibited slightly

lower and more stable values, typically between 0.50 and 0.55. The marginal reduction and improved stability in friction for the larger pin diameter can be attributed to more uniform load distribution and the formation of a stable tribolayer at the contact interface.

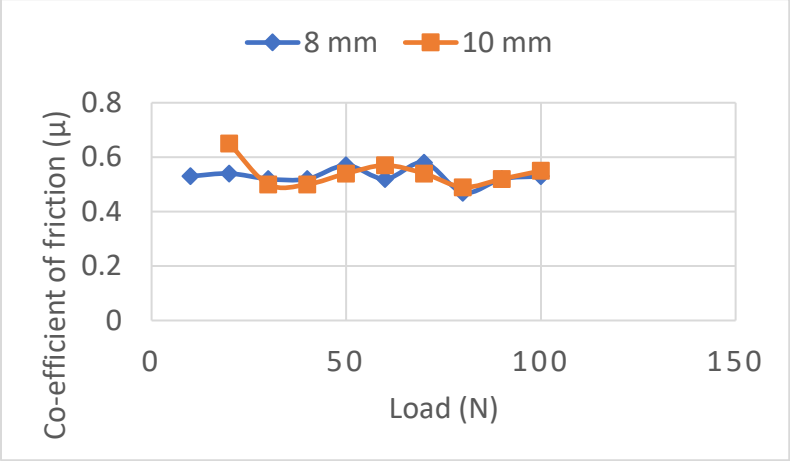

Figure 12: Comparison of co-efficient of friction vs load for 10 mm specimen at 1 m/s

The superimposed plot of the dimensionless wear coefficient against load is presented in Figure 13. Higher wear coefficient values were observed at lower loads for both pin diameters, corresponding to the running-in wear regime characterized by unstable asperity interactions. At low loads (10–20 N), the wear coefficient for the 8 mm pin was approximately 6.6×10^{-5}, whereas for the 10 mm pin it was around 3.3×10^{-5}. With increasing load, the wear coefficient decreased and stabilized for both specimens, remaining in the range of $(2.5–4.0) \times 10^{-5}$ at higher loads. The consistently lower wear coefficient of the 10 mm pin further confirms its superior resistance to material removal under identical operating conditions.

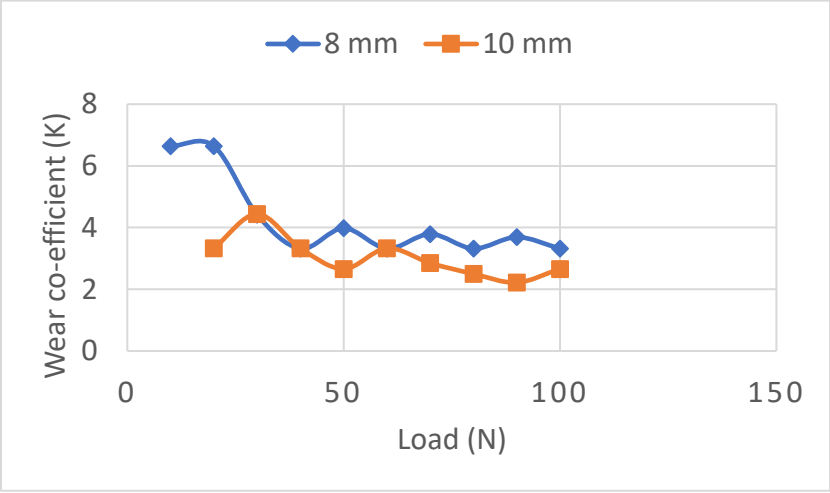

Figure 13: Comparison of wear co-efficient vs load for 10 mm specimen at 1 m/s

Overall, the superimposed graphical analysis clearly demonstrates that increasing pin diameter enhances wear performance by reducing contact stress, leading to lower wear rate, improved frictional stability, and reduced wear coefficient. While the governing wear mechanism remains unchanged for both specimens, specimen geometry plays a critical role in controlling the severity of wear in Al–Mg_2Si composites under dry sliding conditions.

5. Conclusions

The dry sliding wear behavior of in-situ Al–Mg_2Si metal matrix composites was systematically investigated at a constant sliding velocity of 1 m/s under varying applied loads. The results demonstrate that applied normal load is the dominant factor influencing wear rate, which increases monotonically due to enhanced real contact area and plastic deformation at the sliding interface. In contrast, the specific wear rate remains nearly constant across the load range, confirming adherence to Archard's wear law and indicating a stable wear mechanism.

The coefficient of friction exhibits minimal sensitivity to load, suggesting steady-state sliding behavior facilitated by the formation of a stable tribolayer. Comparative analysis of pin geometry reveals that larger diameter pins offer improved wear resistance and reduced wear coefficients due to lower contact stress. Overall, the findings confirm that in-situ Al–Mg_2Si composites possess excellent wear resistance and stable tribological performance under low sliding velocity conditions, making them suitable for moderate-load engineering applications.

References

1. Miracle DB. Metal matrix composites – From science to technological significance. *Compos Sci Technol.* 2005;65(15–16):2526–2540.
2. Surappa MK. Aluminium matrix composites: Challenges and opportunities. *Sadhana.* 2003;28(1–2):319–334.
3. Kainer KU. *Metal Matrix Composites: Custom-made Materials for Automotive and Aerospace Engineering.* Weinheim: Wiley-VCH; 2006.
4. Lloyd DJ. Particle reinforced aluminium and magnesium matrix composites. *Int Mater Rev.* 1994;39(1):1–23.
5. Rohatgi PK. Cast aluminum–matrix composites for automotive applications. *JOM.* 1991;43(4):10–15.
6. Hashim J, Looney L, Hashmi MSJ. Metal matrix composites: Production by the stir casting method. *J Mater Process Technol.* 1999;92–93:1–7.
7. Zhang J, Fan T, Ding J, Zhang D. Microstructure and wear properties of in situ Al–Mg_2Si composites. *Mater Sci Eng A.* 2007;456(1–2):43–51.
8. Wu Y, Liao H, Li J. Dry sliding wear behavior of Al–Mg_2Si composites. *Wear.* 2011;271(9–10):2198–2205.
9. Anilkumar HC, Hebbar HS, Ravishankar KS. Mechanical properties of fly ash reinforced aluminium alloy composites. *Wear.* 2008;265(1–2):97–104.
10. Prasad SV, Asthana R. Aluminum metal–matrix composites for automotive applications: Tribological considerations. *Tribol Int.* 1997;30(1):49–60.

11. Suresh S. *Fatigue of Materials.* 2nd ed. Cambridge: Cambridge University Press; 1998.
12. Archard JF. Contact and rubbing of flat surfaces. *J Appl Phys.* 1953;24(8):981–988.
13. Lim SC, Ashby MF. Wear-mechanism maps. *Wear.* 1995;181–183:12–21.
14. Hutchings IM. *Tribology: Friction and Wear of Engineering Materials.* London: Butterworth-Heinemann; 1992.
15. Akhlaghi F, Zare-Bidaki A. Influence of graphite content on dry sliding and oil impregnated sliding wear behavior of Al–Si–graphite composites. *Wear.* 2005;259(7–12):843–851.
16. Alpas AT, Embury JD. Sliding and abrasive wear behaviour of an aluminium (2014)–SiC composite. *Wear.* 1992;155(1):83–104.
17. Pradeep L, Keshavamurthy R, Rao BN. Wear behavior of aluminum metal matrix composites. *Mater Des.* 2011;32(8–9):4283–4289.
18. Rohatgi PK, Asthana R, Das S. Solidification, structures, and properties of cast metal–ceramic particle composites. *Metall Mater Trans A.* 1991;22(6):143–152.
19. Straffelini G, Bonollo F, Molinari A. Wear of aluminum alloys under dry sliding conditions. *Wear.* 2001;249(1–2):192–198.
20. Das S. Development of aluminium alloy composites for engineering applications. *Tribol Int.* 2004;37(7):573–584.
21. Baradeswaran A, Elaya Perumal A. Influence of B_4C on the tribological and mechanical properties of Al 7075–B_4C composites. *Compos Part B.* 2014;56:464–471.
22. Holm R. *Electric Contacts: Theory and Application.* Berlin: Springer; 1946.
23. Sarkar AD. *Wear of Metals.* Oxford: Pergamon Press; 1976.
24. Stachowiak GW, Batchelor AW. *Engineering Tribology.* 4th ed. Oxford: Elsevier; 2014.
25. Prasad BK. Sliding wear response of zinc-based alloys and composites. *Wear.* 2001;250(1–12):1361–1370.
26. Kumar S, Subramanya Sarma V. Effect of load and sliding speed on wear behaviour of aluminium matrix composites. *Wear.* 2013;303(1–2):35–44.
27. Basavarajappa S, Chandramohan G, Mukund K, Ashwin M, Prabu M. Dry sliding wear behavior of Al 2219/SiC metal matrix composites. *Wear.* 2007;262(7–8):1007–1012.
28. Shorowordi KM, Laoui T, Haseeb ASMA, Celis JP, Froyen L. Microstructure and interface characteristics of B_4C, SiC and Al_2O_3 reinforced Al matrix composites. *Wear.* 2009;266(11–12):113–121.
29. Alaneme KK, Bodunrin MO. Mechanical behaviour of alumina reinforced aluminium matrix composites. *Mater Des.* 2011;32(7):1177–1185.
30. Zhang S, Wang F. Comparison of friction and wear performance of steel–steel and steel–ceramic pairs. *Tribol Lett.* 2010;40(2):227–235.